Published in final edited form as:

Hypertension. 2021 February ; 77(2): 605–616. doi:10.1161/HYPERTENSIONAHA.120.14858.

Nanoscale study of calcium handling remodeling in right ventricular cardiomyocytes following pulmonary hypertension.

Roman Medvedev, PhD[1,2,3], **Jose L. Sanchez-Alonso, PhD**[2], **Anita Alvarez-Laviada, PhD**[2], **Stefano Rossi, PhD**[4], **Eef Dries, PhD**[2,5], **Tilo Schorn, PhD**[3], **Vahitha B. Abdul-Salam, PhD**[2], **Natalia Trayanova, PhD**[6], **Beata Wojciak-Stothard, PhD**[2], **Michele Miragoli, PhD**[3,4], **Giuseppe Faggian, MD**[1], **Julia Gorelik, PhD**[2]

[1]Dipartimento di Cardiochirurgia, Università degli Studi di Verona, Ospedale Borgo Trento, P.le Stefani 1, 37126 Verona, Italy

[2]Department of Cardiovascular Sciences, National Heart and Lung Institute, Imperial College London, Du Cane Road London W12 0NN, United Kingdom

[3]Humanitas Clinical and Research Center, Via Manzoni 56, 20090 Rozzano, Italy.

[4]Dipartimento di Medicina e Chirurgia, Università degli Studi di Parma, Via Gramsci 14, 43124 Parma, Italy

[5]Lab of Experimental Cardiology, University of Leuven, Herestraat 49 box 911, Leuven, Belgium

[6]Department of Biomedical Engineering and Alliance for Cardiovascular Diagnostic and Treatment Innovation; Johns Hopkins University; Baltimore, MD, 21218; USA

Abstract

Pulmonary hypertension is a complex disorder characterized by pulmonary vascular remodeling and right ventricular hypertrophy, leading to right heart failure. The mechanisms underlying this process are not well understood. We hypothesize that the structural remodeling occurring in the cardiomyocytes of the right ventricle affects the cytosolic Ca^{2+} handling leading to arrhythmias. After 12 days of monocrotaline-induced pulmonary hypertension in rats epicardial mapping showed electrical remodeling in both ventricles. In myocytes isolated from the hypertensive rats, a combination of high-speed camera and confocal line-scan documented a prolongation of Ca^{2+} transients along with a higher local Ca^{2+}-release activity. These Ca^{2+} transients were less synchronous than in controls, likely due to disorganized transverse-axial tubular system. In fact, following pulmonary hypertension, hypertrophied right ventricle myocytes showed significantly reduced number of transverse tubules and increased number of axial tubules; however, STED microscopy demonstrated that the co-localization of L-type Ca^{2+} channels and RyR2 remained unchanged. Finally, STED microscopy and super resolution scanning patch-clamp analysis uncovered a decrease in the density of active L-type Ca^{2+} channels in RV myocytes with an elevated open probability of the T-tubule anchored channels. This may represent a general

Address for correspondence: Julia Gorelik, PhD, Department of Cardiovascular Sciences, National Heart and Lung Institute, 4th floor, Imperial Centre for Translational and Experimental Medicine, Hammersmith Campus, Imperial College London, Du Cane Road, London W12 0NN, United Kingdom Tel.: 44(0)2075942736, Fax: 44(0)20 7594 3653, j.gorelik@ic.ac.uk.

Disclosures

None.

mechanism of how nanoscale structural changes at the early stage of pulmonary hypertension impact on the development of the end stage failing phenotype in the right ventricle.

Graphical Abstract

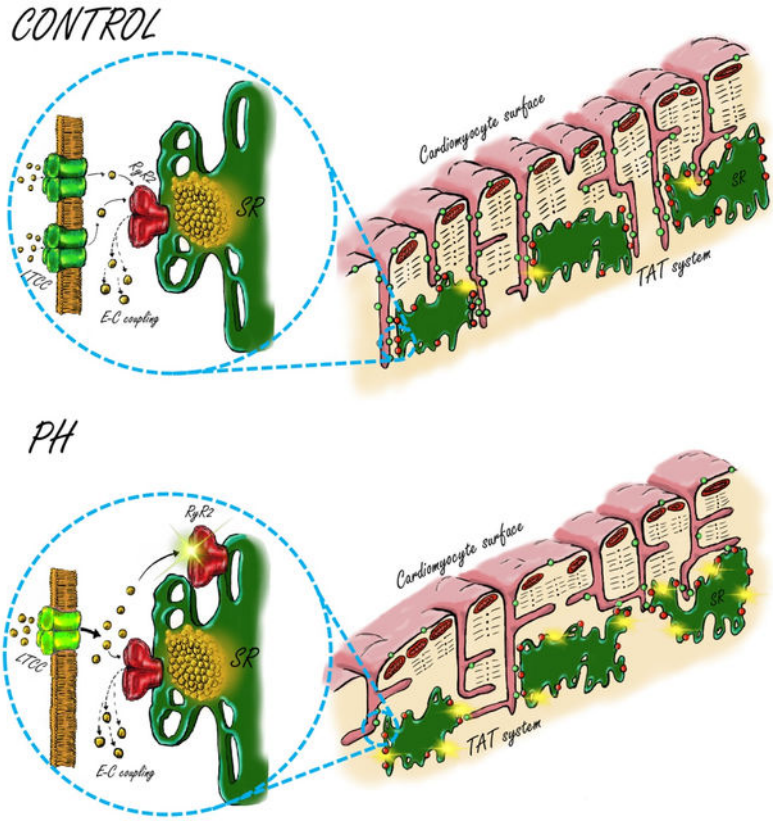

Keywords

right ventricle; cardiomyocytes; electrical remodeling; T-tubule; Ca^{2+} sparks; L-type Ca^{2+} channels

Subject codes

Pulmonary hypertension; Hypertrophy; Calcium Cycling; Excitation-Contraction Coupling; Ion Channels/Membrane Transport

INTRODUCTION

Pulmonary arterial hypertension (PAH) is a vascular disease induced by increased proliferation of cells in the pulmonary vasculature, leading to progressive narrowing of the vascular lumen and increased workload of the right ventricle (RV).[1] PAH patient survival is largely determined by the ability of the RV to adapt to the pressure overload.[2] In PAH, the RV undergoes structural[3] and electrical remodeling.[4,5] Even though the PAH-induced changes in the RV are known, so far there is no specific RV targeted treatment. While

treatments effective for the left ventricular (LV) hypertrophy have been proposed for the RV dysfunction[1], the differences in the biological origin and working conditions of the two chambers[6] raise questions about the suitability of such approach. A better understanding of the mechanisms of RV remodeling in PAH is clearly needed.

RV hypertrophy has been studied by different groups using a monocrotaline induced model of pulmonary hypertension (PH) in rats.[7–9] This model reproduces several important aspects of the cellular and molecular remodeling linked to human PAH pathogenesis.[10] At the level of Ca^{2+} handling some discrepancies have been found, with some groups finding smaller and slower Ca^{2+} transients,[9,11] and others observing an increase in Ca^{2+} transients and more intensive contractions in myocytes.[7,8] Furthermore, alterations in Ca^{2+} transients have been linked to structural changes in the transverse-axial tubular system (TATS).[9,12] Specifically, in PH RV myocytes, it has been shown that the increase in spontaneous Ca^{2+} releases could be due to a reduction of SERCA2a pump expression and activity.[7] Interestingly, considering the importance of L-type Ca^{2+} channels (LTCC) in the Ca^{2+} handling process, no alteration in expression or whole cell current was reported in PH RV myocytes.[7,13]

These described changes in Ca^{2+} signaling could be due to the reorganization in the microdomains. Recently we reported that microdomain remodeling in the failing human and rat LV myocytes could produce the arrhythmogenic triggers that lead to reentrant arrhythmias.[14] Microdomain organization in ventricular myocytes is maintained by the elaborate organization of TATS, bringing LTCCs close to ryanodine receptors (RyR2) and establishing an excitation-contraction coupling. The loss of TATS in heart failure (HF) has been associated with the redistribution of functional LTCCs from T-tubule to sarcolemma membrane[14] and with the uncoupling of sarcoplasmic reticulum from the sarcolemma membrane.[15] The redistribution of the LTCCs is accompanied by an increased open probability,[14,16] likely due to the channel hyperphosphorylation of the channels. Although this is well described in LV myocytes, little is known about the microdomain organization of RV myocytes and their changes during RV failure. We hypothesized that RV myocytes have less complex organization of the excitation-contraction coupling microdomains compared to LV myocytes due to the lower workload of the chamber, and that in PH the microdomain remodeling leads to relocation and hyperactivation of LTCCs.

In this study we evaluated in an early stage of PH, the functional and structural changes in RV and LV myocytes at nanoscale level that could be responsible for the altered cardiac electrophysiology seen in pre-clinical models of PH. We have identified prominent cytoarchitectural changes at the single cell level, from the TATS regularity to the surface topography. Our approach allowed us to distinct two subpopulations of LTCC and RyR2 in RV cardiomyocytes; one located close to the T-tubules and one away from them. Hyperactivation of T-tubular LTCC in conjunction with SR RyR2 coupling could be responsible for the high spontaneous Ca^{2+} releases, desynchronization of Ca^{2+} transients and appearance of alternans in PH hearts.

METHODS

The data supporting the results presented in this article is available from the corresponding authors upon reasonable request. Detailed descriptions of animal procedures, cell isolation, and other methodologies are available in the Online Supplement (please see http://hyper.ahajournals.org). This work was approved by the Animal Welfare and Ethics Review Board (AWERB) of Imperial College London. It is guided by United Kingdom Home Office guidelines (ASPA 1986 and EU Directive 2010/83). The monocrotaline model of PH was generated in male Sprague-Dawley rats by 60 mg/kg intraperitoneal injection,[17] with the experiments performed on days 10–12 after injection. Epicardial mapping with 11×11 multielectrode grid was applied to analyze electrical properties of the tissue.[18] Standard procedures were applied to measure the conduction velocity (CV), excitability, refractoriness, and mean parameters of ECG.[19,20] Cell isolation was performed using a modified Landendorf perfusion protocol.[21] Data analysis was performed using GraphPad prism 6. Normality was assessed by the Kolmogorov–Smirnov test. In cases where data failed the normality test, the nonparametric Kruskal-Wallis analysis of variance (ANOVA) with Dunn's post-hoc analysis was used instead of the two-way ANOVA test with Bonferroni post-hoc comparison. Fisher exact test was used for the occurrence analysis of extrasystole, Ca^{2+} transient alternans and the analysis of LTCC density. All data were expressed as mean ± standard error of mean (SEM). A value of $p<0.05$ was considered statistically significant.

RESULTS

Early stage PH rat characterization, RV hypertrophy with conduction abnormalities

PH monocrotaline (MCT) treated rats showed a significant increase in the mean pulmonary artery pressure within 12 days of MCT injection (Figure 1B), which was accompanied by a higher lung weight (Figure S1B) and muscularization (Figure S1C and S1D). RV hypertrophy was indicated by a markedly increased ratio of RV to LV/septum weight in PH rats (Figure 1C), as previously reported in this model.[7,8]

The electrophysiological properties of RV and LV control and PH rats were studied by epicardial multiple lead recording. The multielectrode grid and representative isochrone maps measured in RV and LV are presented in Figures S2 and S3A, respectively. PH led to a decrease in conduction velocity along epicardial fiber direction longitudinally (CV-l) in both ventricles, but only statistically significant in LV tissue ($p<0.05$, Figure S3B). We found no changes in conduction velocity across epicardial fiber direction transversally (CV-t) in both RV and LV after PH (Figure S3C). Interestingly, when the CV-l/CV-t was calculated to measure the anisotropy ratio of conduction velocity (Figure 1D), it showed a lower value in PH rats and only statistically significant in RV ($p<0.05$). The refractoriness of the tissue was assessed with the analysis of the effective refractory period (ERP). In control animals, the ERP in RV was significantly shorter than in LV ($p<0.01$, Figure 1E). PH led to a prolongation of ERP both in the RV ($p<0.01$) and the LV ($p<0.05$). The basic electrocardiogram parameters were also evaluated (Figure S4). We found longer QT intervals in the LV compared with the RV ($p<0.001$) and the RV in PH showed prolonged QT with respect to that in control RV ($p<0.05$, Figure S4C).

The arrhythmogenicity of the tissue was assessed by the occurrence of extrasystoles. We recorded a higher number of animals with extrasystoles in the PH group, 5 out of 7 animals, versus 3 out of 7 animals in the control group, but this difference was not statistically significant (Figure 1F).

Increased local Ca^{2+} transients in PH RV cardiomyocytes promotes Ca^{2+} alternans.

To evaluate Ca^{2+} handling in PH rat myocytes, we analyzed the spontaneous Ca^{2+} waves by optical mapping according to [22]. Two types of waves were examined, local and propagated through the entire cell, as shown in Figure 2A. The frequency of local waves was significantly elevated in PH RV myocytes ($p<0.05$, Figure 2C) without changes in the frequency of propagated waves (Figure S5). Local Ca^{2+} releases were then analyzed using the line mode of the confocal microscope.[23] A representative Ca^{2+} spark image is shown in Figure 2B. In the control group, RV myocytes showed a similar frequency of Ca^{2+} sparks as LV myocytes (Figure 2D), but spark mass was lower in RV myocytes (Figure 2E). In the PH group, RV myocytes exhibited a significant increase in Ca^{2+} spark frequency (Figure 2E) and mass (Figure S5B) as compared to the control group. These properties of Ca^{2+} sparks were preserved in PH LV myocytes. Elevated rate of Ca^{2+} sparks could be associated with elevated SR Ca^{2+} load or abnormal SERCA2a Ca^{2+} reuptake. However, caffeine–induced Ca^{2+} release experiments did not show significant changes in fractional Ca^{2+} release and SERCA2a activity (Figure S6).

Abnormal Ca^{2+} cycling has been shown to be associated with the appearance of Ca^{2+} transients alternans.[24] When single cardiomyocytes were paced at 4 Hz, the proportion of cardiomyocytes showing Ca^{2+} transient alternans in PH RV myocytes were significantly higher than in control RV myocytes (Figure 2E).

To examine the effects of the increased spontaneous local Ca^{2+} activity in PH RV myocytes, we performed analysis of the electrically evoked Ca^{2+} transients (Figures 3A and S7). Ca^{2+} transients of significantly slower time to peak were observed in PH RV myocytes (Figure 3B). Next, the spatial variability of time to reach half-maximal fluorescence (TTF50) across the cell was analyzed. Histograms of TTF50 in LV myocytes have a peak around 10 ms, whereas for RV myocytes the peak is lower and the distribution is wider (Figures S8A and S8B). A ‘dyssynhcrony index’ defined as the standard deviation of TTF50,[25] showed a significantly higher value in PH RV myocytes as compared to control RV myocytes (Figure 3C).

We used the approach of Heinzel et al[26] and Biesmans et al[27] to divide Ca^{2+} release points into early and late ones according to their TTF50 (Figure S8C). We used 50% of the cumulative histogram as a threshold value for this division (Figure S8D). Ca^{2+} sparks occurring in early or delayed areas were analyzed separately. In PH RV myocytes, Ca^{2+} spark duration and time to peak in delayed areas were significantly prolonged (Figures 3D and S9G). Ca^{2+} sparks from delayed areas had a higher frequency and amplitude in PH RV myocytes but not in PH LV myocytes (Figure S9A-S9F).

Structural regularity is reduced in PH RV myocytes.

It has been shown previously that the reorganization of membrane structure affects the Ca^{2+} handling and synchronization in the LV myocytes.[25,28,29] To study the organization of the sarcolemma membrane, TATS and surface topography of RV and LV myocytes were visualized by Di-8-ANEPPS membrane staining and SICM, respectively. Representative images are shown in Figure 4A. In analyzing the cardiomyocytes shape the length to width ratio was decreased in PH RV myocytes ($p<0.01$, Figure 4B). RV myocytes from PH rats had a reduced length (Figure S10A) and increased width (Figure S10B) compared to control ones, while LV myocytes became thinner in PH (Figure S10B).

In the analysis of SICM images, we used the z-groove ratio as an index of surface regularity[30] and found a significant z-groove index reduction in RV myocytes in PH (Figure 4C) as compared to control. However, despite this reduction, the number of T-tubule openings on the surface of PH myocytes was unaffected (Figure S10C).

Although the total density of the TATS was preserved in PH rats (Figure S10D), the average TATS regularity was reduced in PH RV cardiomyocytes (Figure 4D). The directional analysis of TATS[31] showed a re-arrangement of tubules from the transversal to the axial direction in PH, which could explain the differences in the regularity (Figure 4E). The average fraction of the axial tubules was significantly higher in PH RV myocytes as compared to control (Figure 4F), whereas the average fraction of transverse tubules was significantly lower (Figure 4F).

RV cardiomyocytes exhibit smaller $Ca_V1.2$ density

We hypothesized that remodeling of the TATS in PH leads to dissociation of LTCC from RyR2, which could be the cause for the Ca^{2+} handling changes mentioned above. It has been shown that in HF, orphaned RyR2 are the source of increased spontaneous Ca^{2+} activity.[32] To determine the amount of LTCC co-localized with RyR2, we performed Stimulation Emission Depletion (STED) imaging on fixed myocytes. Figure 5A illustrates representative STED images of RV and LV myocytes stained with antibodies against $Ca_V1.2$ (magenta) and RyR2 (cyan). There were no differences in $Ca_V1.2$ and RyR2 signal densities between control RV and LV myocytes (Figure 5B and 5C). PH promoted a reduction of $Ca_V1.2$ signal density in RV myocytes, but not in LV ones (Figure 5B). No alterations in signal density of RyR2 staining were found in PH (Figure 5C). These results were supported by Western blot analysis (Figure S11). While a trend towards a reduction of Cav1.2 protein expression in RV tissue after PH (Figure S11B), no changes were observed in the levels of RyR2 protein expression in RV tissue after PH (Figure S11D).

Co-localization of $Ca_V1.2$ and RyR2 was determined using two methods: by defining the percentage of overlap between the two stainings and by calculating Manders' coefficients.[33,34] The colocalization analysis did not show any significant changes in both parameters: percentages of overlapped Cav1.2 or RyR2 (Figure 5D and 5E) and Manders coefficients (Figure S12).

Open probability of L-type Ca^{2+} channels in the T-tubules of RV cardiomyocytes is increased in PH.

Finally, to understand the localization and distribution of functionally active LTCC in RV myocytes in the context of functional changes in the PH heart, we used super resolution patch clamp method (Figure 6). LTCC membrane density is calculated by normalizing the total number of channels observed in TT or crest to the patched area.[35,36] It has been shown that in LV myocytes LTCCs predominantly localize in T-tubules and not in the crest area.[28,37] However, in RV myocytes LTCCs were observed at almost equal density in both locations; only a slightly (not significant) higher channel density was found in T-tubule versus crest microdomains (Figure 6C). Inlet in Figure 6C shows that PH RV myocytes have a reduced density of functional LTCCs, however no significant changes were found regarding LTCCs in T-tubules or crests. To maximize the chance of recording LTCC current, we applied the LTCC agonist BayK8644 in the next set of experiments (Figure 6B). In the presence of BAYK8644 in control myocytes the average density of LTCC in control and PH myocytes remained equal (Figure 6D).

We then calculated the open probability of LTCC in all the groups. In control RV myocytes, the open probability (Po) of LTCC was significantly lower in the T-tubules as compared to the crest (Figure 6E). In PH RV myocytes, the LTCCs located in T-tubules exhibited a significantly elevated Po in respect to control T-tubules ($p<0.05$), with the crest subpopulation of LTCCs having preserved Po after PH. In the presence of BayK8644, the mean LTCC Po was preserved (Figure S13).

DISCUSSION

This study provides evidence of the nanoscale microdomain-related disruptions in Ca^{2+} handling that occur in PH, which could affect electrical conductance in the heart. We conclude that during PH development, the increased workload of RV due to the high pulmonary artery pressure causes structural remodeling of TATS and surface topography in RV myocytes. This structural remodeling promotes local alterations in the Po of LTCC and in the frequency and duration of delayed Ca^{2+} sparks, which in turn could be responsible for the desynchronization of Ca^{2+} transients and the appearance of Ca^{2+} transient alternans observed. The increase in local spontaneous Ca^{2+} activity and the appearance of Ca^{2+} transient alternans could serve as trigger for arrhythmias in the settings of substantial tissue remodeling.[38] However, our *in vivo* experiments showed that the remodeling is not sufficient to evoke a significant arrhythmic activity, as reported at the more severe stages of disease.[7] In LV myocytes, PH leads to prolongation of Ca^{2+} transients but this occurs without changes in TATS organization.

PH induced RV hypertrophy and electrical remodeling

It was previously shown that PH leads to RV hypertrophy formation of arrhythmogenic substrates at the last stages of disease.[7] Here we studied the preceding changes in electrical remodeling. The increase of CV anisotropic ratio was linked to the generation of unidirectional conduction block and sink to source mismatch.[39] Our data shows that that early PH leads to the reduction in the anisotropy ratio in RV but not in LV (Figure 1D). It

has also been known that structural remodeling of the tissue influences CV.[40] However, it has been already shown previously that no significant increases in fibrosis, apoptosis or infiltration of the inflammatory cells occur in the heart tissue after 2 weeks of MCT treatment.[41] On the other hand, RV myocytes in PH become significantly hypertrophied (Figure 4B) and redistribution of gap junction occurs[40] on the surface of PH RV myocytes; these changes can produce alteration of the passive electrical properties of the ventricle and change the balance between longitudinal and transverse conductions.

We also observed longer ERP in both RV and LV following PH (Figure 1E), which could be related to the prolonged Ca^{2+} transient duration (Figure 3B and Figure S7). Increasing the ERP can precipitate *torsades de pointes*, a type of ventricular tachycardia caused by early or delayed afterdepolarizations.[42] We did not see a significant increase in occurrence of extrasystole in the PH RV as compared to the control RV, so we could assume this stage of the disease is not severe enough for the development of a pro-arrhythmogenic substrate.

The observed remodeling of LV electrophysiology and cell dimensions could be induced by neurohormonal activation in PH hearts[43] or due to mechanical interdependence of the two ventricles.[44]

PH increased spontaneous Ca^{2+} activity in RV myocytes

PH led to an increase in spontaneous local Ca^{2+} waves and Ca^{2+} sparks frequency in RV but not LV myocytes. Interestingly, the preserved SR Ca^{2+} load and SERCA activity in PH myocytes suggest the remodeling happens mostly in RyR2 activity. We observed a significantly slower time to peak of Ca^{2+} transients in PH RV myocytes (Figure 3B), with an increased Ca^{2+} transient dyssynchronization (Figure 3C). Dyssynchronization of Ca^{2+} transients found in PH RV myocytes could be related to the rearrangement of TATS.

We defined the early and delayed Ca^{2+} release points of Ca^{2+} transients according to their TTF50 (Figure S9). Early release regions of Ca^{2+} transients were shown to arise from areas with higher TAT density while delayed ones arose from areas with lower TATS density.[26] Assigning of Ca^{2+} sparks to early or delayed areas were performed according to their position on the scan line. RV myocytes showed a significantly higher frequency of early sparks versus delayed ones (Figure S9). Higher frequency of sparks located close to the T-tubule has been shown in myocytes from different species.[27,45] It has been proposed that the higher local Ca^{2+} concentration close to the T-tubule produces Ca^{2+} sparks more frequently. PH significantly increased the frequency and prolonged the duration of delayed but not the early Ca^{2+} sparks in RV myocytes. This could be due to rearrangement of the TATS microdomains or alterations of RyR2 clustering. Kolstad et al[46] showed that in failing LV myocytes RyR2 undergo significant dispersion and that large RyR2 clusters produce slower Ca^{2+} sparks and, consequently, a desynchronization of Ca^{2+} transients.

Ca^{2+} transient alternans observed in PH RV myocytes could be related to the abnormal Ca^{2+} release or Ca^{2+} reuptake (Figure 2F). As we did not find any reduction in SERCA activity in PH (Figure S6), the appearance of Ca^{2+} alternans could be associated with the abnormal RyR2 activity.[47] Ca^{2+} transient alternans have been shown to produce action potential duration alternans, reentrant activity and contractile impairment,[24] however, our *in vivo* data

indicates that the remodeling was still not sufficient for the formation of a pro-arrhythmic substrate (Figure 1).

TATS reorganization in PH

TATS organization largely impacts on the intracellular Ca^{2+} cycling.[25] We observed a reduction of TATS power of regularity in RV PH myocytes due to the lower amount of transverse tubules and a higher number of axial tubules in PH (Figure 4). The recent study by Shobesberger et al[48] documented higher frequency of axial (longitudinal) tubules during hypertrophic state of the myocardial infarction. The role of axial elements in the excitation-contraction coupling is still not fully understood, although recent studies of Ashari et al[49] and Swift et al[50] showed that axial tubules can be fully functional with LTCC coupled to SR and RyR2 clusters. Thus, the increase in the number of axial tubules was proposed to be the first compensatory mechanism in maintaining high working load and secure Ca^{2+} influx to support contractions.[50]

Analysis of the membrane topography by SICM showed a reduction in z-groove index in RV but not in LV myocytes in PH (Figure 4C). Studies of LV myocytes from rat and human failing hearts have shown that this reduction is accompanied by an increase of Ca^{2+} waves and sparks.[14,28] The disruption of surface topography could be linked with the weakening of sarcomeres and myocardial stretch, which results in opening of stretch-activated channels,[8] and/or altered Ca^{2+}– troponin interaction at different sarcomere lengths.[51]

RV $Ca_v1.2$ re-arrangement in PH

Our results on PH rats showed that RyR2 protein expression and RyR2 STED signal densities are unchanged when compared to control (Figure S11 and 5C). In agreement with this, research into HF and PH has demonstrated that RyR2 arrangement and expression is preserved in failing myocytes.[8,9] RyR2 activation depends on the Ca^{2+} entry through LTCC. Interestingly, we observed the distribution of LTCC between T-tubule and crest in RV is more similar to atrial myocytes than LV myocytes.[14,22,37] Taking into account differences observed in early and delayed Ca^{2+} sparks parameters between control RV and LV myocytes, these findings suggest an altered organization of Ca^{2+} handling microdomains between both ventricles.

Following PH, we found a reduction of $Ca_v1.2$ STED signal density (Figure 5B) and a reduction in the number of functional LTCCs in RV myocytes (Figure 6C). The analysis of $Ca_v1.2$ protein expression from tissue after PH (Figure S11) and the LTCC density in presence of agonist (Figure 6D), however, did not show a significant change. Also, co-localization between RyR2 and $Ca_v1.2$ in both RV and LV myocytes was not affected by PH (Figure 5D). This evidence suggests that the expression of Cav1.2 protein remains unaffected at this early stage of the disease, but a functional remodeling of LTCC is already happening. This is supported by other groups that found no changes of the pore-forming $Ca_v1.2$ protein expression in the early hypertrophic stage of the disease.[7,13] Although a down-regulation of $Ca_v1.2$ protein expression has been observed in the late stages of PH.[9,52] In terms of whole-cell Ca^{2+} current, which density in PH RV myocytes is preserved,[7] we suggest that the silencing of functional LTCCs is partially compensated by the increase of

the Po in T-tubular LTCC. This increased Po of LTCC in T-tubules could be caused by phosphorylation of the channels by PKA or CaMKII.[14,16] In fact, Fowler et al[12] found an increased β-adrenergic stimulation in PH rats, which will activate PKA and consequently, LTCCs. Although this activation could work as a compensatory mechanism to keep the contraction requirements, it could also be the substrate of the increased Ca^{2+} activity observed in this work. Overall, our findings underscore the role of nanoscale organization of Ca^{2+} handling within myocytes in the pathophysiology of the heart, particularly during development of a disease such as PH.

Perspectives

Our study shows that during development of PH RV cardiomyocytes undergo structural remodeling that induces functional alterations of intracellular Ca^{2+} behavior and could affect the electrical properties of the whole heart. However, the arrhythmogenic activity in the RV, reported at the later stages of PH, was not found. This suggests that the changes observed at the cellular level could precede development of arrhythmias. Our findings provide new mechanistic insights into right ventricular dysfunction, which could help identify novel therapeutic approaches for RV failure in PH.

Supplementary Material

Refer to Web version on PubMed Central for supplementary material.

Acknowledgments

We thank Peter O'Gara for myocyte isolation.

Sources of funding

This work was supported by British Heart Foundation grants (RG/17/13/33173 to JG and PG/15/69/31719 to B.W.-S) and NIH grant (ROI-HL 126802 to NT and JG).

REFERENCES

1. Handoko ML, De Man FS, Allaart CP, Paulus WJ, Westerhof N, Vonk-Noordegraaf A. Perspectives on novel therapeutic strategies for right heart failure in pulmonary arterial hypertension: Lessons from the left heart. Eur Respir Rev. 2010;19(115):72–82. doi:10.1183/09059180.00007109 [PubMed: 20956170]
2. Thenappan T, Ormiston ML, Ryan JJ, Archer SL. Pulmonary arterial hypertension: Pathogenesis and clinical management. BMJ. 2018;360:54–92. doi:10.1136/bmj.j5492
3. Bogaard HJ, Abe K, Noordegmaf AV, Voelkel NF. The right ventricle under pressure. Chest. 2009;135(3):794–804. doi:10.1378/chest.08-0492 [PubMed: 19265089]
4. Hlaing T, DiMino T, Kowey PR, Yan GX. ECG repolarization waves: Their genesis and clinical implications. Ann Noninvasive Electrocardiol. 2005;10(2):211–223. doi:10.1111/j.1542-474X.2005.05588.x [PubMed: 15842434]
5. Folino AF, Bobbo F, Schiraldi C, Tona F, Romano S, Buja G, Bellotto F. Ventricular Arrhythmias and Autonomic Profile in Patients with Primary Pulmonary Hypertension. Lung. 2003;181(6):321–328. doi:10.1007/s00408-003-1034-x [PubMed: 14749936]
6. Haddad F, Hunt SA, Rosenthal DN, Murphy DJ. Right ventricular function in cardiovascular disease, part I: Anatomy, physiology, aging, and functional assessment of the right ventricle. Circulation. 2008;117(11):1436–1448. doi:10.1161/CIRCULATIONAHA.107.653576 [PubMed: 18347220]

7. Benoist D, Stones R, Drinkhill MJ, Benson AP, Yang Z, Cassan C, Gilbert SH, Saint DA, Cazorla O, Steele DS, Bernus O, White E. Cardiac arrhythmia mechanisms in rats with heart failure induced by pulmonary hypertension. Am J Physiol Hear Circ Physiol. 2012;302:2381–2395. doi:10.1152/ajpheart.01084.2011-Pulmonary
8. Sabourin J, Boet A, Rucker-Martin C, Lambert M, Gomez AM, Benitah JP, Perros F, Humbert M, Antigny F. Ca^{2+} handling remodeling and STIM1L/Orai1/TRPC1/TRPC4 upregulation in monocrotaline-induced right ventricular hypertrophy. J Mol Cell Cardiol. 2018;118(April):208–224. doi:10.1016/j.yjmcc.2018.04.003 [PubMed: 29634917]
9. Xie YP, Chen B, Sanders P, Guo A, Li Y, Zimmerman K, Wang LC, Weiss RM, Grumbach IM, Anderson ME, Song LS. Sildenafil prevents and reverses transverse-tubule remodeling and Ca^{2+} handling dysfunction in right ventricle failure induced by pulmonary artery hypertension. Hypertension. 2012;59(2):355–362. doi:10.1161/HYPERTENSIONAHA.111.180968 [PubMed: 22203744]
10. Ryan JJ, Huston J, Kutty S, Hatton ND, Bowman L, Tian L, Herr JE, Johri AM, Archer SL. Right ventricular adaptation and failure in pulmonary arterial hypertension. Can J Cardiol. 2015;31(4):391–406. doi:10.1016/j.cjca.2015.01.023 [PubMed: 25840092]
11. Kuramochi T, Honda M, Tanaka K, Enornoto K-i, Hashimoto M, Morioka S. Ca2+ Transients in Single Myocytes and Membranous Ultrastructures During the Development of Cardiac Hypertrophy and Heart Failure in Rats. Clin Exp Pharmacol Physiol. 1994;21(12):1009–1018. doi:10.1111/j.1440-1681.1994.tb02664.x [PubMed: 7736651]
12. Fowler ED, Drinkhill MJ, Norman R, Pervolaraki E, Stones R, Steer E, Benoist D, Steele DS, Calaghan SC, White E. Beta1-adrenoceptor antagonist, metoprolol attenuates cardiac myocyte Ca^{2+} handling dysfunction in rats with pulmonary artery hypertension. J Mol Cell Cardiol. 2018;120(May):74–83. doi:10.1016/j.yjmcc.2018.05.015 [PubMed: 29807024]
13. Rocchetti M, Sala L, Rizzetto R, Staszewsky LI, Alemanni M, Zambelli V, Russo I, Barile L, Cornaghi L, Altomare C, Ronchi C, Mostacciuolo G, Lucchetti J, Gobbi M, Latini R, Zaza A. Ranolazine prevents I_{NaL} enhancement and blunts myocardial remodelling in a model of pulmonary hypertension. Cardiovasc Res. 2014;104(1):37–48. doi:10.1093/cvr/cvu188 [PubMed: 25139747]
14. Sanchez-Alonso JL, Bhargava A, O'Hara T, Glukhov AV., Schobesberger S, Bhogal N, Sikkel MB, Mansfield C, Korchev YE, Lyon AR, Punjabi PP, Nikolaev VO, Trayanova NA, Gorelik J. Microdomain-Specific Modulation of L-Type Calcium Channels Leads to Triggered Ventricular Arrhythmia in Heart Failure. Circ Res. 2016;119(8):944–945. doi:10.1161/CIRCRESAHA.116.308698 [PubMed: 27572487]
15. Zhang C, Chen B, Guo A, et al. Microtubule-mediated defects in junctophilin-2 trafficking contribute to myocyte transverse-tubule remodeling and Ca^{2+} handling dysfunction in heart failure. Circulation. 2014;129(17):1742–1750. doi:10.1161/CIRCULATIONAHA.113.008452 [PubMed: 24519927]
16. Bryant SM, Kong CHT, Watson J, Cannell MB, James AF, Orchard CH. Altered distribution of ICa impairs Ca^{2+} release at the t-tubules of ventricular myocytes from failing hearts. J Mol Cell Cardiol. 2015;86:23–31. doi:10.1016/j.yjmcc.2015.06.012 [PubMed: 26103619]
17. Abdul-Salam VB, Russomanno G, Chien-Nien C, Mahomed AS, Yates LA, Wilkins MR, Zhao L, Gierula M, Dubois O, Schaeper U, Endruschat J, Wojciak-Stothard B. CLIC4/Arf6 Pathway. Circ Res. 2019;124(1):52–65. doi:10.1161/CIRCRESAHA.118.313705 [PubMed: 30582444]
18. Savi M, Bocchi L, Rossi S, et al. Antiarrhythmic effect of growth factor-supplemented cardiac progenitor cells in chronic infarcted heart. Am J Physiol Circ Physiol. 2016;310(11):H1622–H1648. doi:10.1152/ajpheart.00035.2015
19. Rossi S, Baruffi S, Bertuzzi A, Miragoli M, Corradi D, Maestri R, Alinovi R, Mutti A, Musso E, Sgoifo A, Brisinda D, Fenici R, Macchi E. Ventricular activation is impaired in aged rat hearts. Am J Physiol Circ Physiol. 2008;295(6):H2336–H2347. doi:10.1152/ajpheart.00517.2008
20. Carnevali L, Trombini M, Rossi S, Graiani G, Manghi M, Koolhaas JM, Quaini F, MacChi E, Nalivaiko E, Sgoifo A. Structural and electrical myocardial remodeling in a rodent model of depression. Psychosom Med. 2013;75(1):42–51. doi:10.1097/PSY.0b013e318276cb0d [PubMed: 23257930]

21. Sato M, O'Gara P, Harding SE, Fuller SJ. Enhancement of adenoviral gene transfer to adult rat cardiomyocytes in vivo by immobilization and ultrasound treatment of the heart. Gene Ther. 2005;12(11):936–941. doi:10.1038/sj.gt.3302476 [PubMed: 15759019]
22. Glukhov AV, Balycheva M, Sanchez-Alonso JL, Ilkan Z, Alvarez-Laviada A, Bhogal N, Diakonov I, Schobesberger S, Sikkel MB, Bhargava A, Faggian G, Punjabi PP, Houser SR, Gorelik J. Direct evidence for microdomain-specific localization and remodeling of functional L-type calcium channels in rat and human atrial myocytes. Circulation. 2015;132(25):2372–2384. doi:10.1161/CIRCULATIONAHA.115.018131 [PubMed: 26450916]
23. Picht E, Zima AV, Blatter LA, Bers DM. SparkMaster: automated calcium spark analysis with ImageJ. AJP Cell Physiol. 2007;293(3):C1073–C1081. doi:10.1152/ajpcell.00586.2006
24. Laurita KR, Rosenbaum DS. Cellular mechanisms of arrhythmogenic cardiac alternans. Prog Biophys Mol Biol. 2008;97(2–3):332–347. doi:10.1016/j.pbiomolbio.2008.02.014 [PubMed: 18395246]
25. Louch WE, Mørk HK, Sexton J, Strømme TA, Laake P, Sjaastad I, Sejersted OM. T-tubule disorganization and reduced synchrony of Ca^{2+} release in murine cardiomyocytes following myocardial infarction. J Physiol. 2006;574(2):519–533. doi:10.1113/jphysiol.2006.107227 [PubMed: 16709642]
26. Heinzel FR, Bito V, Volders PGA, Antoons G, Mubagwa K, Sipido KR. Spatial and temporal inhomogeneities during Ca^{2+} release from the sarcoplasmic reticulum in pig ventricular myocytes. Circ Res. 2002;91(11):1023–1030. doi:10.1161/01.RES.0000045940.67060.DD [PubMed: 12456488]
27. Biesmans L, Macquaide N, Heinzel FR, Bito V, Smith GL, Sipido KR. Subcellular heterogeneity of ryanodine receptor properties in ventricular myocytes with low T-tubule density. PLoS One. 2011;6(10). doi:10.1371/journal.pone.0025100
28. Lyon AR, MacLeod KT, Zhang Y, Garcia E, Kanda GK, Lab MJ, Korchev YE, Harding SE, Gorelik J. Loss of T-tubules and other changes to surface topography in ventricular myocytes from failing human and rat heart. Proc Natl Acad Sci. 2009;106(16):6854–6859. doi:10.1073/pnas.0809777106 [PubMed: 19342485]
29. Litwin SE, Zhang D, Bridge JHB. Dyssynchronous Ca^{2+} sparks in myocytes from infarcted hearts. Circ Res. 2000;87(11):1040–1047. doi:10.1161/01.RES.87.11.1040 [PubMed: 11090550]
30. Gorelik J, Yang LQ, Zhang Y, Lab M, Korchev Y, Harding SE. A novel Z-groove index characterizing myocardial surface structure. Cardiovasc Res. 2006;72(3):422–429. doi:10.1016/j.cardiores.2006.09.009 [PubMed: 17054929]
31. Wagner E, Lauterbach MA, Kohl T, et al. Stimulated Emission Depletion Live-Cell Super-Resolution Imaging Shows Proliferative Remodeling of T-Tubule Membrane Structures After Myocardial Infarction. New Methods Cardiovasc Biol Stimul. 2012;111(4):402–414. doi:10.1161/CIRCRESAHA.112
32. Song L-S, Sobie EA, McCulle S, Lederer WJ, Balke CW, Cheng H. Orphaned ryanodine receptors in the failing heart. Proc Natl Acad Sci. 2006;103(11):4305–4310. doi:10.1073/pnas.0509324103 [PubMed: 16537526]
33. Bolte S, Martin CFP, Cordelières FP. A guided tour into subcellular colocalization analysis in light microscopy. J Microsc. 2006;224(3):213–232. doi:10.1111/j.1365-2818.2006.01706.x [PubMed: 17210054]
34. Gilles JF, Dos Santos M, Boudier T, Bolte S, Heck N. DiAna, an ImageJ tool for object-based 3D co-localization and distance analysis. Methods. 2017;115:55–64. doi:10.1016/j.ymeth.2016.11.016 [PubMed: 27890650]
35. Novak P, Gorelik J, Vivekananda U, Shevchuk AI, Ermolyuk YS, Bailey RJ, Bushby AJ, Moss GWJ, Rusakov DA, Klenerman D, Kullmann DM, Volynski KE, Korchev YE. Nanoscale-Targeted Patch-Clamp Recordings of Functional Presynaptic Ion Channels. Neuron. 2013;79(6):1067–1077. doi:10.1016/j.neuron.2013.07.012 [PubMed: 24050398]
36. Poulet C, Sanchez-Alonso J, Swiatlowska P, Mouy F, Lucarelli C, Alvarez-Laviada A, Gross P, Terracciano C, Houser S, Gorelik J. Junctophilin-2 tethers T-tubules and recruits functional L-type calcium channels to lipid rafts in adult cardiomyocytes. Cardiovasc Res. 2020;(cvaa033). doi:10.1093/cvr/cvaa033

37. Bhargava A, Lin X, Novak P, Mehta K, Korchev Y, Gorelik J. Super-resolution scanning patch clamp reveals clustering of functional ion channels in adult ventricular myocyte. Circ Res. 2013;112(8):1112–1120. doi:10.1161/CIRCRESAHA.111.300445 [PubMed: 23438901]
38. Venetucci LA, Trafford AW, O'Neill SC, Eisner DA. The sarcoplasmic reticulum and arrhythmogenic calcium release. Cardiovasc Res. 2008;77(2):285–292. doi:10.1093/cvr/cvm009 [PubMed: 18006483]
39. Van Rijen HVM, Eckardt D, Degen J, Theis M, Ott T, Willecke K, Jongsma HJ, Opthof T, De Bakker JMT. Slow Conduction and Enhanced Anisotropy Increase the Propensity for Ventricular Tachyarrhythmias in Adult Mice with Induced Deletion of Connexin43. Circulation. 2004;109(8):1048–1055. doi:10.1161/01.CIR.0000117402.70689.75 [PubMed: 14967725]
40. Uzzaman M, Honjo H, Takagishi Y, Emdad L, Magee AI, Severs NJ, Kodama I, Honjo H, Takagishi Y, Emdad L, Magee AI, Severs NJ. Remodeling of gap junctional coupling in hypertrophied right ventricles of rats with monocrotaline-induced pulmonary hypertension. Circ Res. 2000;86(8):871–878. doi:10.1161/01.RES.86.8.871 [PubMed: 10785509]
41. Deng Y, Wu W, Guo S, Chen Y, Liu C, Gao X, Wei B. Altered mTOR and Beclin-1 mediated autophagic activation during right ventricular remodeling in monocrotaline-induced pulmonary hypertension. Respir Res. 2017;18(1). doi:10.1186/s12931-017-0536-7
42. Volders PGA, Sipido KR, Vos MA, Spätjens RLHMG, Leunissen JDM, Wellens HJJ. Downregulation of delayed rectifier K^+ currents in dogs with chronic complete atrioventricular block and acquired torsades de pointes. Circulation. 1999;100(24):2455–2461. doi:10.1161/01.CIR.100.24.2455 [PubMed: 10595960]
43. Brunner F Cardiac endothelin and big endothelin in right-heart hypertrophy due to monocrotaline-induced pulmonary hypertension in rat. Cardiovasc Res. 1999;44(1):197–206. doi:10.1016/S0008-6363(99)00155-8 [PubMed: 10615403]
44. Lamberts RR, Vaessen RJ, Westerhof N, Stienen GJM. Right ventricular hypertrophy causesimpairment of left ventricular diastolicfunction in the rat. Basic Res Cardiol. 2007;102(1):19–27. doi:10.1007/s00395-006-0620-5 [PubMed: 16944361]
45. Meethal SV, Potter KT, Redon D, Munoz-del-Rio A, Kamp TJ, Valdivia HH, Haworth RA. Structure-function relationships of Ca^{2+} spark activity in normal and failing cardiac myocytes as revealed by flash photography. Cell Calcium. 2007;41(2):123–134. doi:10.1016/j.ceca.2006.05.006 [PubMed: 16837043]
46. Kolstad TR, van den Brink J, Macquaide N, Lunde PK, Frisk M, Aronsen JM, Norden ES, Cataliotti A, Sjaastad I, Sejersted OM, Edwards AG, Lines GT, Louch WE. Ryanodine receptor dispersion disrupts Ca2+ release in failing cardiac myocytes. Elife. 2018;7:1–24. doi:10.7554/eLife.39427
47. Pieske B, Kockskämper J. Alternans goes subcellular: A "disease" of the ryanodine receptor? Circ Res. 2002;91(7):553–555. doi:10.1161/01.RES.0000036862.37203.F4 [PubMed: 12364380]
48. Schobesberger S, Wright P, Tokar S, Bhargava A, Mansfield C, Glukhov AV., Poulet C, Buzuk A, Monszpart A, Sikkel M, Harding SE, Nikolaev VO, Lyon AR, Gorelik J. T-tubule remodelling disturbs localized β2-adrenergic signalling in rat ventricular myocytes during the progression of heart failure. Cardiovasc Res. 2017;113(7):770–782. doi:10.1093/cvr/cvx074 [PubMed: 28505272]
49. Asghari P, Schulson M, Scriven DRL, Martens G, Moore EDW. Axial tubules of rat ventricular myocytes form multiple junctions with the sarcoplasmic reticulum. Biophys J. 2009;96(11):4651–4660. doi:10.1016/j.bpj.2009.02.058 [PubMed: 19486687]
50. Swift F, Franzini-Armstrong C, Oyehaug L, Enger UH, Andersson KB, Christensen G, Sejersted OM, Louch WE. Extreme sarcoplasmic reticulum volume loss and compensatory T-tubule remodeling after Serca2 knockout. Proc Natl Acad Sci. 2012;109(10):3997–4001. doi:10.1073/pnas.1120172109 [PubMed: 22355118]
51. Lab MJ, Allen DG, Orchard CH. The effects of shortening on myoplasmic calcium concentration and on the action potential in mammalian ventricular muscle. Circ Res. 1984;55(6):825–829. doi:10.1161/01.RES.55.6.825 [PubMed: 6499137]
52. Benoist D, Stones R, Drinkhill M, Bernus O, White E. Arrhythmogenic substrate in hearts of rats with monocrotaline-induced pulmonary hypertension and right ventricular hypertrophy. Am J

Physiol Heart Circ Physiol. 2011;300(6):H2230–7. doi:10.1152/ajpheart.01226.2010 [PubMed: 21398591]

Novelty and Significance

What Is New?

- We observed that at an early stage of pulmonary hypertension, myocytes of right ventricle develop local nanoscale changes in L-type calcium channel and Ca^{2+} spark properties which could encourage dysregulation of Ca^{2+} transients which in turn could form a pro-arrhythmic substrate in the whole heart.

What Is Relevant?

- We found alterations in transverse and axial tubular network and surface topography of myocytes, leading to changes in local L-type calcium channel activity and Ca^{2+} spark properties, which occurred before a significant arrhythmogenic remodeling in the whole heart.

Summary

Right ventricle myocytes of the heart have a distinct ultrastructure and functional behavior as compared to left ventricle myocytes. Pulmonary hypertension induces membrane remodeling in right ventricle myocytes and alteration of the local properties of L-type calcium channels and Ca^{2+} sparks, producing significantly altered Ca^{2+} transients and prolonged refractoriness on the whole heart level. Left ventricle at this stage of the disease is mostly preserved in terms of its structure and function, but we cannot exclude its involvement at later stages.

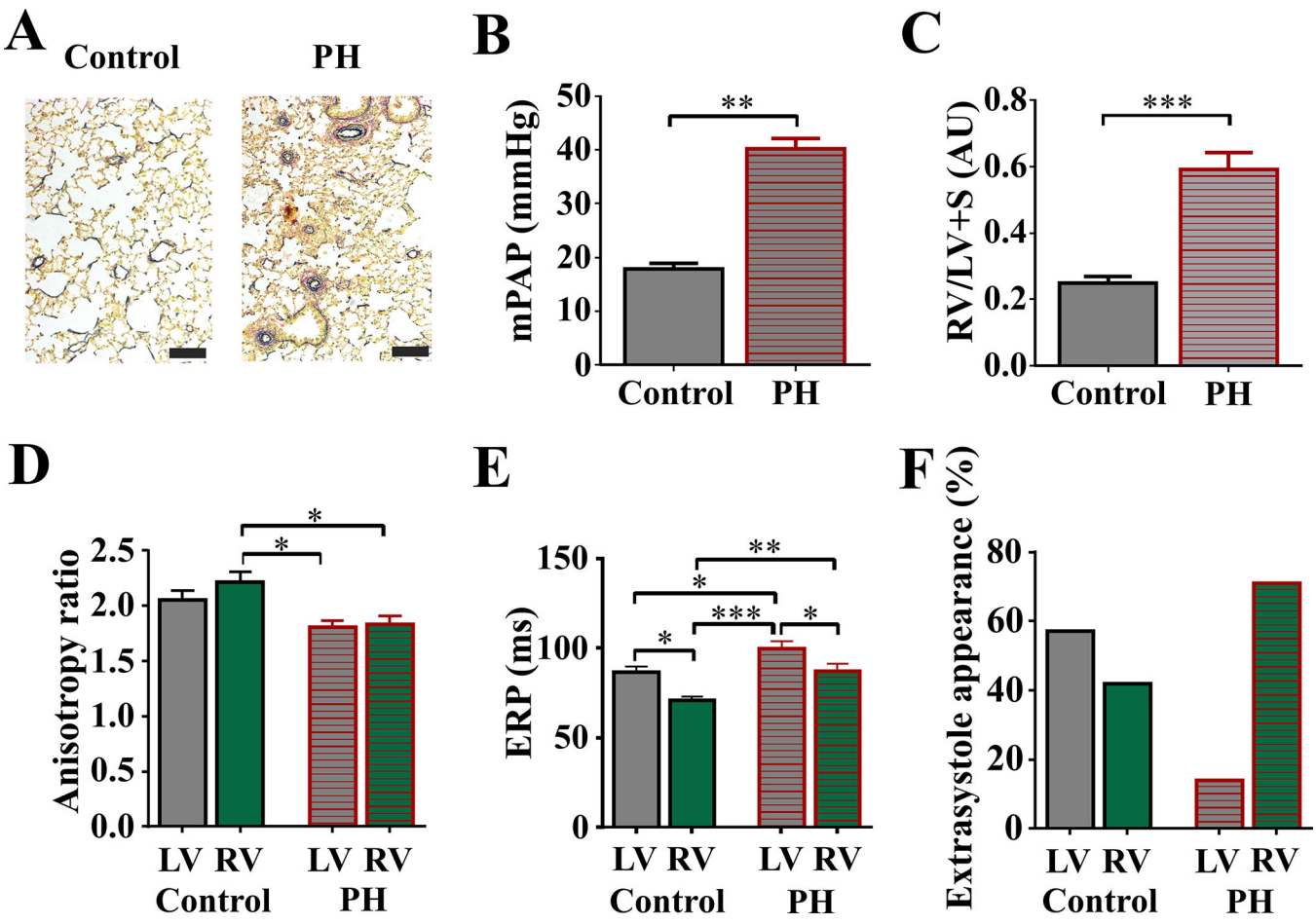

Figure 1. Characterization of control and PH rats.

A) Elastic van Gieson (EVG) representative staining of peripheral arteries in control and MCT treated animals. Scale bar, 100 μm. **B)** Mean pulmonary arterial pressure measured in control and MCT treated rats. **C)** Proportion of RV weight to LV+septum weight in control and MCT treated animals (N=7–12 rats, **p<0.01, ***p<0.001). **D)** Anisotropy ratio averages of conduction velocity (CV-l/CV-t). **E)** Effective refractory period measures. **F)** The percentage of the RV and LV showing extrasystole appearance (N=7 rats, * p<0.05, ** p<0.01).

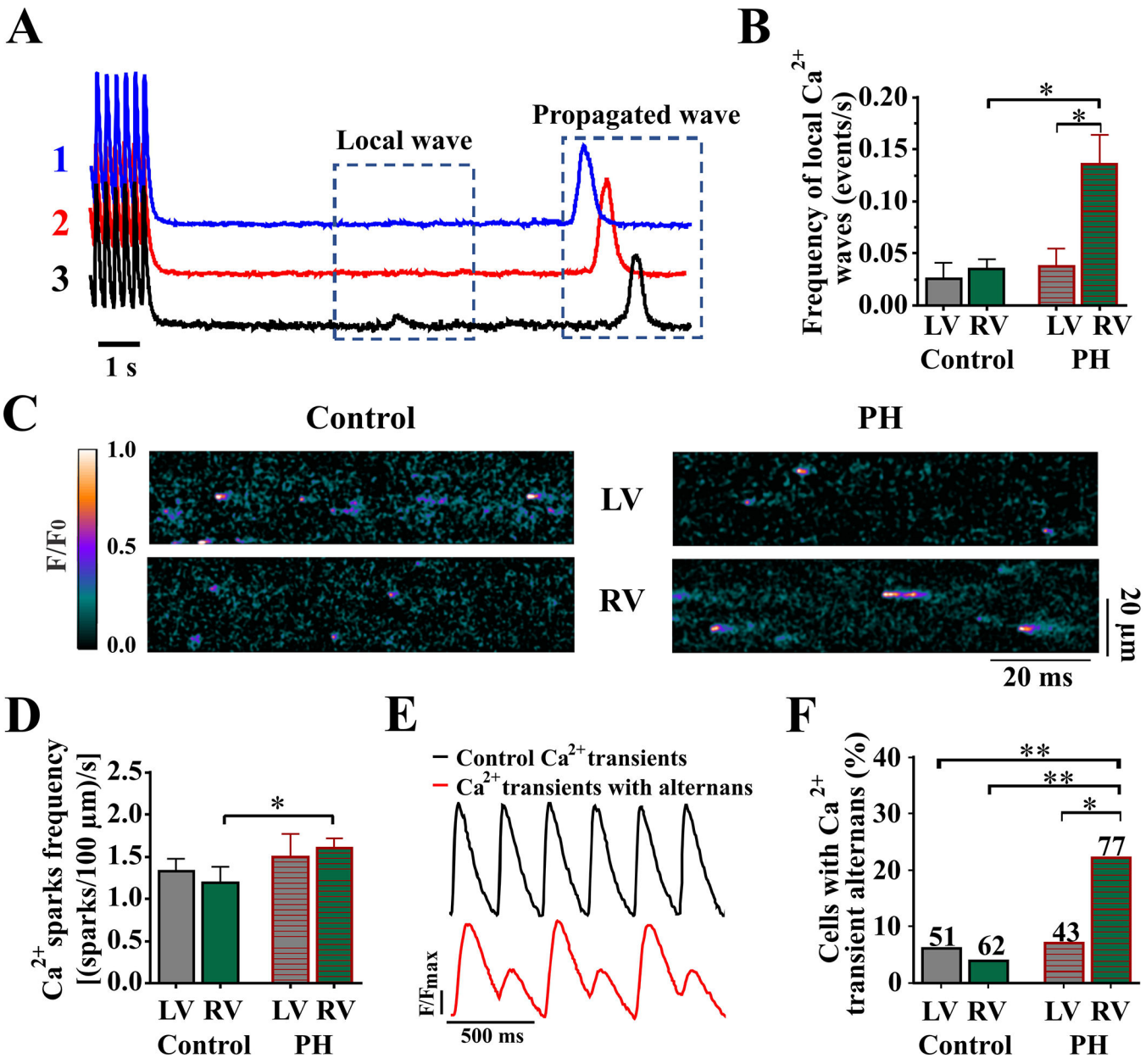

Figure 2. Pulmonary hypertension induced high spontaneous Ca^{2+} activity in RV but not in LV myocytes.

A) Representative traces of spontaneous Ca^{2+} activity measured in isolated ventricular myocytes. Cells were electrically paced at 4 Hz for 1 min to enhance sarcoplasmic reticulum Ca^{2+} loading. Local and propagated Ca^{2+} waves were recorded during a 16-s rest period after cessation of pacing. On the left, optical traces showing changes in [Ca^{2+}] from 3 different points (1–3) selected in a single cardiomyocyte, on the right. **B)** Average frequency of local Ca^{2+} waves (n=25–45 cells, N=5–9 rats, *p<0.05). **C)** Representative confocal line scans of LV (top) and RV (bottom) myocytes loaded with Fluo4-AM. Recordings were performed during 2 s rest period after 1 min of pacing. **D)** Average Ca^{2+} sparks frequency in control and PH myocytes (n=30–67 cells, N=4–5 rats), **E)** Representative traces of Ca^{2+}

transients with and without alternans at 4 Hz stimulation, **F)** The percentage of cells showing Ca^{2+} transients alternans in control and PH myocytes (n=30–67 cells, N=5–6 rats, *p<0.05, **p<0.01).

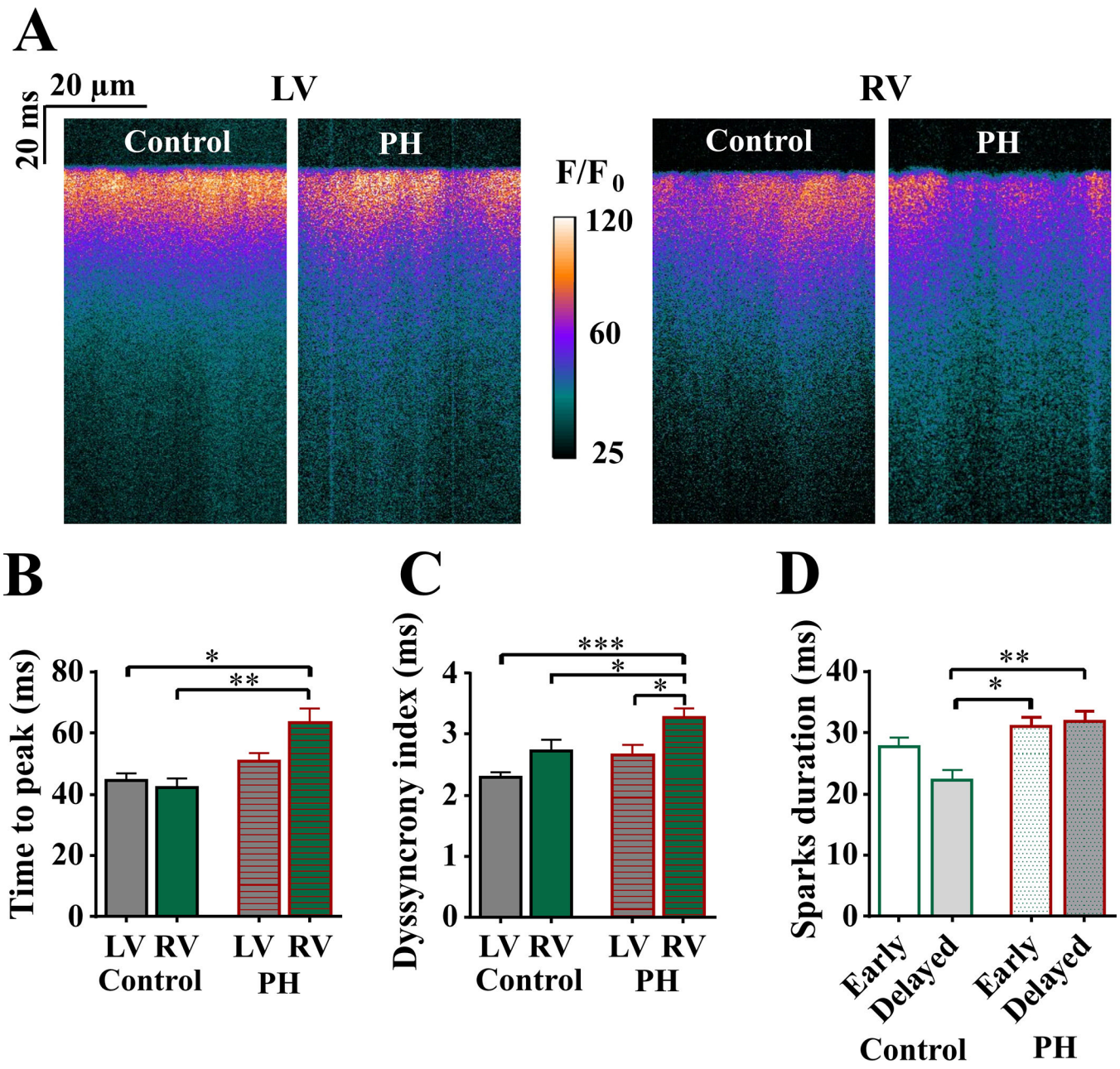

Figure 3. PH – induced desynchronization of Ca^{2+} transients

A) Representative images of Ca^{2+} transients recorded in LV and RV myocytes paced at 1 Hz. **B)** Time to peak of the Ca^{2+} transients measured in LV and RV myocytes from control and PH rats paced at 1Hz (n=14–20 cells, N=4 rats, *p<0.05, **p<0.01). **C)** Average of 'dyssynchrony' index (n=24–38 cells, N=4–5 rats, *p<0.05, *p<0.05, ***p<0.001). **D)** Duration of early and delayed Ca^{2+} sparks measured in control RV and PH RV myocytes. (n=34–41 cells, N=4–5 rats, *p<0.05, **p<0.01).

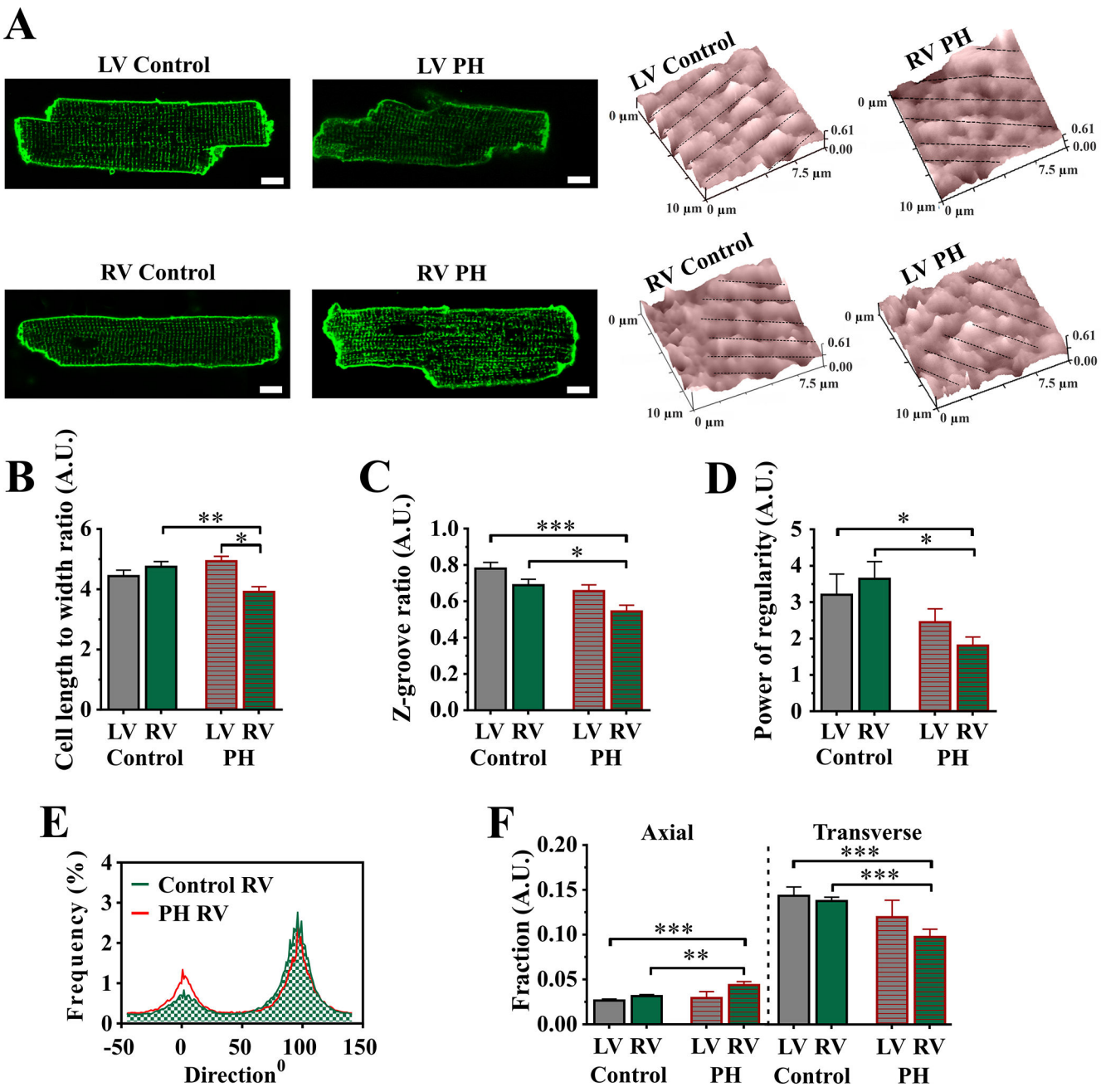

Figure 4. Reorganization of sarcolemma membrane in PH rat model.

A) Representative images of TATS and SICM scans of LV and RV myocytes from control and PH rats; scale bar, 10 µm. **B)** Summary graph of cell length to width ratio (n=37–55 cells. N=4 rats, *p<0.05, **p<0.01). **C)** Average Z-groove ratio of control and PH myocytes (n=23–30 cells, N=3–5 rats, *p<0.05, ***p<0.001). **D)** Power of TATS regularity measured in RV and LV from control and PH myocytes (n=25–40 cells, N=3–5 rats, *p<0.05). **E)** Directionality histograms for the TATS of control and PH RV myocytes and **F)** summary of the axial tubules and transverse tubules in LV and RV myocytes after PH (n=20–73, N=4–5rats, **p<0.01, ***p<0.001).

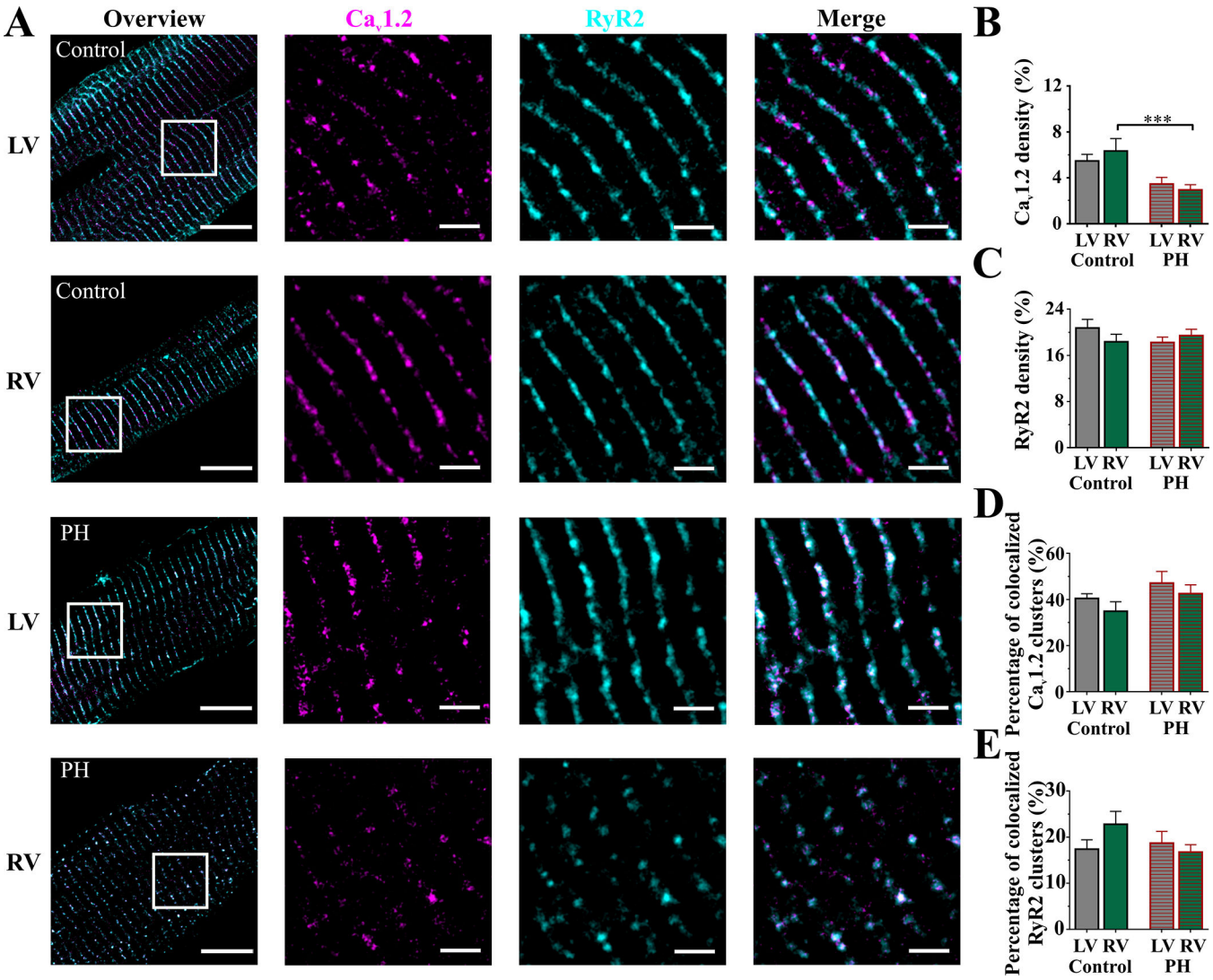

Figure 5. Co-localization of $Ca_v1.2$ and RyR2 in PH rat model.

A) Representative STED confocal images of RV and LV myocytes labelled with antibodies against $Ca_v1.2$ (magenta) and RyR2 (cyan). Overview scale bars: 10 μm. Magnified area scale bars: 2 μm. **B)** Average density of $Ca_v1.2$ signal and **C)** RyR2 signal from LV and RV myocytes from control and PH rats (n=10–16 cells, N=3–4 rats, ***p<0.001). **D)** Percentage of $Ca_v1.2$ clusters colocalized with RyR2 and **E)** Percentage of RyR2 clusters colocalized with $Ca_v1.2$. (n=10–16, N=3–4 rats).

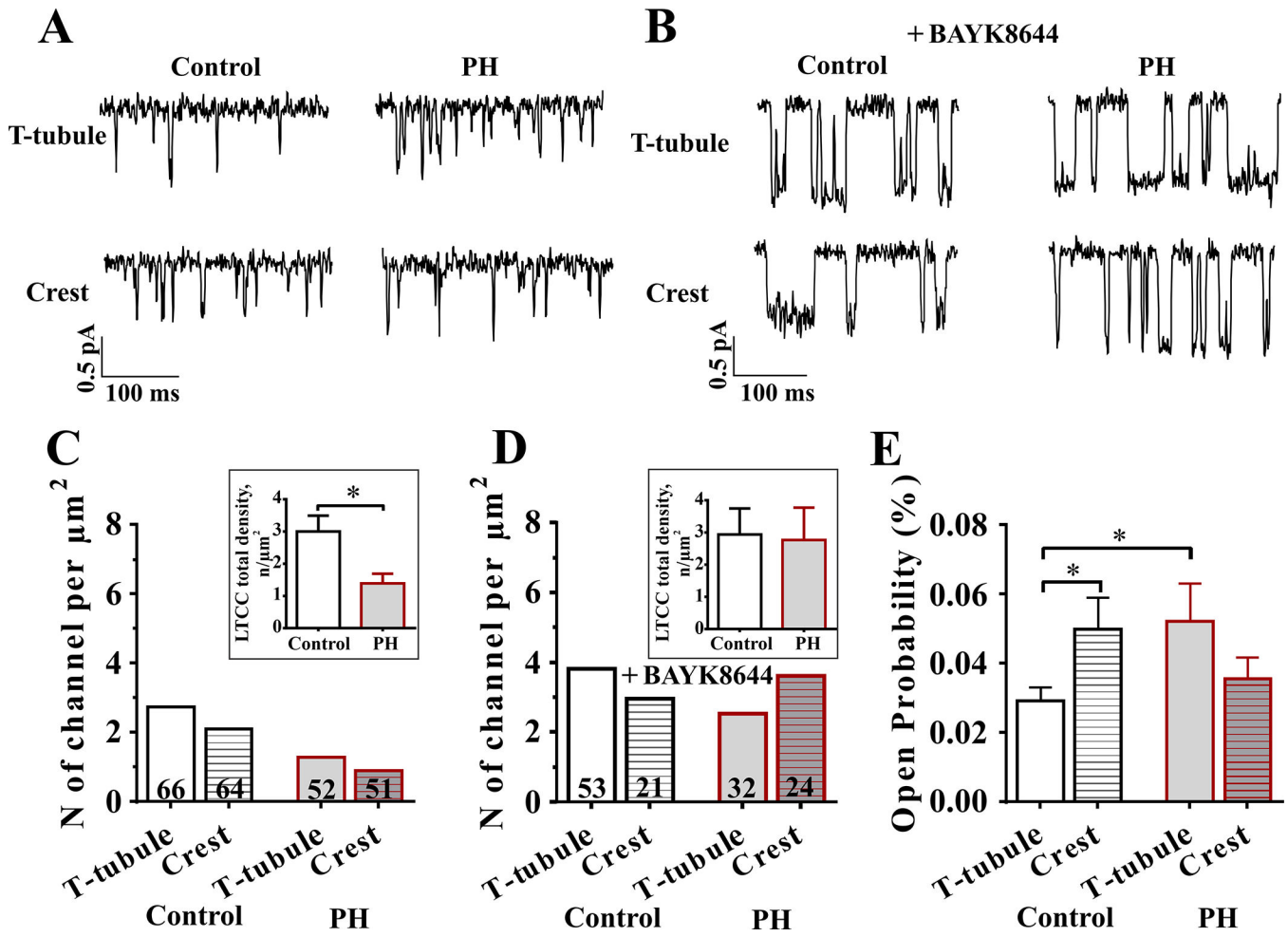

Figure 6. Analysis of L-type Ca^{2+} channels distribution and function in RV myocytes after PH.

A) Representative single channel traces showing LTCC current recorded at −6.7 mV in T-tubule and crests of RV myocytes in normal solution and **B)** in presence of BayK8644. **C)** LTCC density observed in normal solution and **D)** with the agonist in T-tubule and crests of RV myocytes from control and PH rats. The number in each column represents the total number of successful seals in each group. Inlets show total LTCC density analysis from both T-tubules and crests together, from control versus PH RV myocytes. **E)** LTCC open probability (Po) at −6.7 mV in control and PH RV myocytes at physiological conditions or with the agonist BayK8644. (n=6–19 channels, 40–100 cells, 6–10 rats, *p<0.05).